ATOM VERSUS CLUSTER REACTIVITIES FOR CALCIUM AND MAGNESIUM

by

ALAN RAY WHETTEN
//
B.S., Fort Lewis College, 1982

A MASTER'S THESIS

submitted in partial fulfillment of the

requirements for the degree

MASTER OF SCIENCE

Department of Chemistry

KANSAS STATE UNIVERSITY
Manhattan, Kansas

1984

Approved by:

Kenneth J. Klabunde

Major Professor

Acknowledgement

My deepest appreciation is extended to my mother Shirley, my father Al, my brother Paul, and to my wife Barbara and her parents Eva Lee and Robert Hall for their support and encouragement. I would also like to thank Dr. Kenneth Klabunde and my laboratory colleagues for their guidance, patience and friendship during the pursuit of my degree.

TABLE OF CONTENTS

LIST OF TABLES

LIST OF FIGURES

Introduction

Matrix isolation is a technique where a reactive species can be isolated in a frozen matrix at cryogenic temperatures for spectroscopic studies. The active molecules are trapped in a rigid crystalline solvent cage of inert material preventing decomposition and inhibiting diffusion. In this way, intermolecular collisions are stopped or slowed down enough that reactions with an activation energy greater than a few kilojoules per mole cannot occur. Typical matrix temperatures vary from 4.5K to 25K depending on the inert host and type of reaction. Isolation at these temperatures has proven to be very informative in the study of reaction intermediates, free radical species, reaction pathways, and the thermodynamics and kinetics of other transient species which are difficult to prepare and retain for study under more conventional conditions.

Historical

The use of inert gas matrices for spectroscopic study of free radicals was pioneered by G. Porter and G. C. Pimentel and associates[1] in 1954. Subsequently the technique was further developed and utilized by Pimentel's group[2] for infrared studies of the free radical NO_2 and hydrogen bonding molecules in 1956. They reported qualitatively on the success of using Nitrogen, Argon, Xenon, CO_2, CCl_4, and methylcyclohexane as matrix gases. This early study pointed out the importance of inertness, rigidity, transparency and volatility of the matrix material and presented quantitative M/R ratios (moles of matrix gas per moles of metal deposited).

Soon after these initial experiments were performed, the potential of matrix isolation was realized, and a number of important extensions began to appear. Linevsky[3] in 1961 demonstrated the value of trapping high temperature vapors on a frozen matrix. He recorded infrared spectra of lithium fluoride

effusing from a high temperature Knudsen cell and condensing simultaneously with a stream of matrix gas on a window cooled by liquid helium in a double Dewar cryostat. This initiated the use of combining high vaporization materials with the low temperature matrix as a synthetic tool.

In the 1960's, the development of the Joule-Thomson open cycle cryostat allowed better instrument design and more accurate control of the temperature.[4] At this time much research was being done using low temperature condensation of high temperature gaseous species; most notably by Margrave,[5] with gaseous SiF_2, Timms[6] with gaseous boron and silicon subhalides, and Skell[7] with the vaporization of carbon. In 1966, investigations by Andrews and Pimentel[8] led to the production and isolation of alkali metal free radical species. This study and further studies by Andrews[9,10] allowed syntheses for new alkali metal species and made possible the prediction of coordinate geometries of lithium atom-nitric oxide compounds. These early experiments are summarized by the following equations:

$$Li + CH_3I \longrightarrow CH_3 \cdots LiI$$

$$Li + NO \longrightarrow LiON$$

$$Li + O_2 \longrightarrow Li^+ + O_2^-$$

In the last decade, matrix isolation has proven useful in virtually every branch of chemistry. The development of closed cycle cryostats[4] in the early 1970's has made this technique more appealing and relatively facile. Recent contributions to matrix isolation stem from a wide range of interests, including conventional transition metal chemistry,[11,12] organic and organometallic synthesis, homogeneous and heterogeneous catalysis, photochemical reactions, polymerization reactions, metal aggregation phenomena, reactive intermediates, chemisorption, and intermolecular interactions.[13]

With the advancement of better spectroscopic techniques and higher resolv-

ing power of traditional techniques, M.I. has become even more valuable. The reduction of intermolecular interactions in the inert environment produces very sharp monomeric solute absorptions compared to other condensed phase spectra. With the absence of rotational effects, these bands appear much narrower than those obtained in the vapor phase. This has been shown by Reedy,[14] Barnes,[15] and their coworkers to have great potential in the separation and identification of structural and conformational isomers, where there are only small differences between the vibrational spectra of the isomers. Utilizing these enhancements in resolution, M.I. has been combined with laser Raman spectroscopy,[16,17] Mössbauer spectroscopy[18,19] and GC/FTIR spectroscopy.[14] Current state-of-the-art cryochemical apparatus, along with advancements in spectroscopic techniques predicts a promising future for matrix isolation spectroscopy in the scientific research community.

The absorption spectra of calcium codeposited with an inert gas has been studied in several laboratories.[20,21,22] Absorption peaks have been reported in Ar, Kr and Xe matrices. There has been some question over the assignment of some peaks, but it is well established that there is a strong atomic absorption due to the $4s4p\,^1P_1 \longleftarrow 4s^2\,^1S_0$ transition ($^1P_1 \longleftarrow {}^1S_0$) at around 410 nm. This transition appears as an asymmetric doublet corresponding to the 422.6 nm atomic transition in the gas phase. The splitting of this atomic band has been explained as due to the non O_h symmetry of the lattice structure causing a vacancy to be present next to a metal atom.[21] A sharp transition at about 458 nm has been assigned as a forbidden $^1D_2 \longleftarrow {}^1S_0$ atomic Ca transition.[20] It has been suggested that the symmetry of an incompletely substituted matrix site or a site containing a nearby impurity is reduced such that ^1P and ^1D have a common irreducible representation of approximately D_{3h} symmetry. Upon lowering the symmetry (from O_h), these two sites can mix

to give some observable intensity to the forbidden transition.[20] Thus absorptions are seen due to nonequilibrium lattice sites as compared to the unperturbed matrix. This theory was based on concentration studies which indicated a monomer species, and because of the close correspondence to the gas phase $^1D_2 \leftarrow\!\!- \; ^1S_0$ transition at 457 nm. Recently Miller and coworkers[23] have lent theoretical support in alliance with their own magnetic circular dichroism (MCD) experiments. These assignments have also been bolstered by Bondybey[24] who observed both ^1P and ^1D transitions in the excitation spectrum of Ca atoms while monitoring the ^3P emission.

Dimeric calcium species have been extensively studied in inert gas matrices.[23,25,26,27] These species have generated specific interest since the bonding is attributed wholly to van der Waals interactions between the two calcium atoms.[25] The electronic configurations of the dimers have an equal number of bonding and antibonding electrons resulting in no formal bonding in the ground $((\sigma_g 4s)^2(\sigma_u 4s)^2)$ state. However, several low lying excited states are chemically bound due to excitation of an antibonding electron to a bonding $(\sigma_g 4s)^2(\sigma_u 4s)(\sigma_g 4p)$ orbital.[26] One dimeric species has been observed in an Ar matrix as a structured band with twelve members at approximately 113 cm^{-1} spacings.[27] This transition is designated $^1\Sigma_g^+ \; (^1S+^1S) \rightarrow \; ^1\Sigma_u^+ \; (^1S+^1P)$ and is observed at 648 nm. Two other weaker unstructured absorptions have been assigned as Ca dimers. These peaks are relatively broad and are seen around 500 nm and 374 nm. Evidence for these latter designations comes from absorption and emission spectra along with MCD studies.[23] These absorptions are weak and evidence indicates there is an overlap at 500 nm due to a higher aggregate species. The absorption due to Ca_x is observed at 484 nm. It is seen as a broad peak with medium intensity in the visible spectrum. Table I summarizes the absorptions of calcium species in inert

matrices which have been duplicated with accuracy.[20] In all cases it is recorded that Kr and Xe produce much better matrices than Ar and N_2. This is expected because of the larger sizes of Kr and Xe producing a better fit for the metal atoms and also because of the greater rigidity of these two materials at the cryogenic temperatures.

TABLE I

Absorptions (nm) observed upon codeposition of calcium atoms with inert gases[a]

Ne	Ar	Kr	Xe	Identification
315	318	325	362	unknown
380	374	377	386	Ca_2 ?
–	–	–	403	unknown
404,415	410	420	433	Ca $^1P \longleftarrow {}^1S_0$
453	456	458	461	Ca $^1D \longleftarrow {}^1S_0$
479	484	495	505	Ca_x
505	507	512	520	Ca_x + Ca_2
540	548	559	568	Ca_x
642	646	666	696	Ca_2

[a] Bands measured to the nearest nm.

The study of magnesium in matrix isolation experiments was originally investigated and reported by Schnepp in 1961.[28] Since then, magnesium has been isolated several times in inert matrices.[23,27,29,30] Several transitions have been identified via concentration studies and supported with atomic and molecular absorption spectra.

A Mg atomic transition [$^1P(3s3p) \leftarrow {}^1S(3s^2)$] has been identified in an Ar matrix at 285 nm. It is observed as a triplet structure whose origin has been a subject of debate. The triplet has been attributed to metal-metal interactions,[31] multiple trapping sites,[32] and more recently to Jahn-Teller effects.[33] Andrews and his coworkers[33] have presented magnetic circular dichroism evidence indicating the triplet structure is due to a splitting of the orbital degeneracy of the excited state at a single site. They assumed octahedral site symmetry for Mg atoms and observed a $T_1 \times t_{2g}$ coupling of a noncubic (Jahn-Teller active) mode which lowers the symmetry and produces a triplet splitting. This assignment is partially based on other metal ^1S-^1P transitions exhibiting this effect in an Ar matrix. The assignment is still tenative and they are not leaving out the possibility of a splitting arising because the Mg atom in its ground state is at a site whose symmetry is lower than octehedral (static splitting of the ^1P orbital degeneracy).

Two magnesium dimers have been studied and identified in an Ar matrix.[23,29,30] A broad structured $A^1\Sigma_u^+$ ($^1S + {}^1P$) $\leftarrow X^1\Sigma_g^+$ ($^1S + {}^1S$) dimer band is reported at 370 nm, while a weaker non-structured $^1\pi_u \leftarrow {}^1\Sigma_g$ transition is seen at 263 nm. These assignments are based on concentration studies. As in the calcium case, Mg_2 has a formal zero bond order in its ground $X^1\Sigma_g^+$ electronic state and is bound by van der Waals forces. These weak intermolecular interactions are holding together two neutral atoms in a fashion that is much weaker than a two electron covalent bond. Work by Balfour,[34] however,

indicates these molecules are well behaved and have been characterized in terms of equilibrium bond lengths, vibrational frequency and dissociation energy. The finding of these weakly bonded diatomics prompted the study of heteronuclear diatomics which has resulted in identification of absorptions due to CaMg, BaMg, SrMg, and SrCa.[27]

Several aggregate species have been identified as Mg_x without assignment of the size of the cluster.[27,30] Andrews and coworkers[23] have made specific cluster size assignments on the basis of their concentration studies and magnetic circular dichroism results. MCD studies provide detailed information about magnetic properties and degeneracies of both the ground and excited states involved in electronic transitions. This information has led to definitive assignments of the sizes of certain small clusters. The transition at 344 nm has been designated as a Mg_3 cluster while the absorption at 305 nm has been assigned as Mg_4. The band at 289 nm is still defined as Mg_x and implies cluster size greater than four atoms.

Recently reactions of methyl halides with magnesium atoms have been studied in an Ar matrix. In this work Ault,[35] presents evidence for the insertion of a magnesium atom into a carbon-halogen bond to form unsolvated Grignard species of the type $H_3C{-}{-}M{-}{-}X$. The matrix gas to metal ratio was varied between 100/1 and 1000/1 to study dilution effects. The results of these reactions gave rise to four product bands indicating new chemical species. These product bands were observed for Mg + CH_3I, CH_3Br, and CH_3Cl. It is noted that the overall yield (intensity) of the products was greatest for CH_3I, and substantially decreased upon going to CH_3Br and CH_3Cl. The four product bands are hydrogenic in nature and showed large deuterium isotope shifts. These bands are assigned to the four vibrations of the C_{3v} methyl group in the reaction product (symmetric and antisymmetric C-H stretches,

and symmetric and antisymmetric deformation modes). There is some uncertainty in assigning the carbon-magnesium stretching vibration in the 500 cm^{-1} region, but IR evidence shows that the nature of the halogen in the complex has very little effect on this vibration, indicating the halogen is not directly bound to the carbon. This stretching vibration is however strongly dependent upon the metal atom, indicating a product of the form H_3CMgX.

The previous results were reproduced in our laboratory, and the oxidative addition of CH_3Br was studied using several metals.[36] The high concentrations of Mg metal and the long vaporization times led to the theory and investigation that it could be the Mg clusters and not the atoms which are the reactive species in the frozen matrix.

Our recent investigations examined the reactivity of the atoms, dimers, and clusters of Mg toward CH_3Br.[37] In this study we isolated these species on a KBr crystal and monitored the reactivity using ultraviolet-visible spectroscopy. Considerable evidence gathered indicates that Mg clusters are necessary in order for oxidative addition to occur with CH_3Br under matrix isolation conditions. Jasien and Dykstra,[38] have supported our proposal with their theoretical evidence for strong metal-metal stabilization of H_3CMg_2X species. Their energy comparisons and electronic structure calculations show that there is a consistant 5-6 kcal stabilization that arises from forming a dimagnesium Grignard instead of a simple Grignard.

These results are extremely significant since they appear to be the first examples where a σ-bond breakage is occurring due to the cluster but not the atom under the same experimental conditions. There has been a report of Fe_2 reacting with CH_4 while Fe atoms did not react under identical conditions.[39] These observations, however, have recently been shown to be inaccurate or misinterpreted.[40] The explanations as to the lability of the clusters and

the inertness of the atoms are currently being investigated. These and other studies of the reactivity of atoms vs. clusters toward alkyl halides is the purpose of the present investigation.

Experimental

The matrix isolation unit is modeled after that of Hauge, Kauffman, and Margrave.[41] It is designed so that the matrix chamber can be moved freely into and out of a Beckman IR-12 spectrophotometer and a Cary 14 UV-visible spectrophotometer. The mounting allows both reflectance and absorption/transmission studies to be carried out. The complete design and specifications have been described previously.[42] The unit is cooled by an Air Products Displex closed cycle helium refrigerator, model CSW202. Fine temperature control is possible using an Air Products APD-E Digital Temperature Indicator/Controller. A cold cathode guage and monitor (Kontes/Martin) were used to measure the background pressure. This pressure was approximately 4×10^{-6} torr before vaporization started and maintained around 2×10^{-5} torr during the experiment.

The Furnace was a modified Knudsen cell design. The exact dimensions are illustrated in Figure 1. It was made by cutting a 2 inch x 5/16 inch (outer diameter) pressed Al_2O_3 tube with a wall thickness of 0.05 inches. The tube was then wrapped with 25 micron Ta foil and spot welded along the seam. Next a 1/2 inch (outer diameter) Al_2O_3 sleeve 1 inch long with a 0.055 inch wall thickness was slid over the Ta wrapped tube. This sleeve was also wrapped in 25 micron Ta foil and served as a heat shield to reduce the amount of radiant energy escaping from the furnace. The outer sleeve was centered in the middle of the Al_2O_3 tube. At each end of the furnace there was a 5/16 inch wide piece of 0.5 mm Ta metal which was wrapped around the end of the furnace and spot welded. These served as electrodes for the furnace and extended perpendicular to the furnace axis about 2 inches. The metal used for vaporization was then placed inside the inner Al_2O_3 tube approximately in the center. Each end of the furnace was then fitted with a stain-

less steel plug in which there was a 1.04 mm aperture. These openings allowed metal vapor to escape in one direction toward a cold KBr (25 mm x 4 mm) window which was used for spectroscopic detection, and in the opposite direction toward a quartz crystal microbalance. This microbalance was attached to a digital frequency counter (Data Precision #5845) which allowed quantitative calculations of metal deposited.[43] A chromel-alumel thermocouple was slid between the two Al_2O_3 tubes in the furnace and connected to a type K digital thermometer. The distance from one Knudsen cell effusion hole to the KBr window was 9 cm, and from the other exit to the microbalance was 11 cm.

Figure 1. Knudsen cell furnace used in matrix isolation experiments.

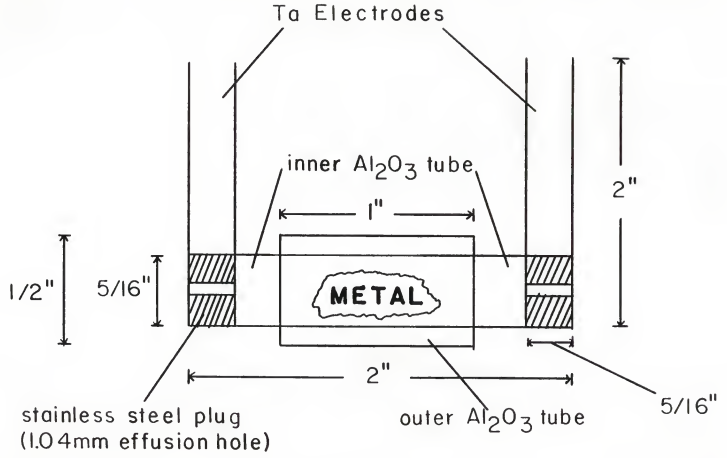
Ta Electrodes
inner Al_2O_3 tube
1"
2"
1/2"
5/16"
METAL
2"
5/16"
stainless steel plug
(1.04mm effusion hole)
outer Al_2O_3 tube

The microbalance is made of a quartz piezoelectric sensor crystal (Airco Temescal model Sc-8009) with a gold plating. The crystal oscillates at a frequency of ≈ 6.0 MHz. As metal deposits on the crystal face, the oscillation frequency decreases. The frequency shift caused by the deposition of metal has been theoretically described by Sauerbrey.[44] The amount of metal deposited on the crystal can be calculated using the following equation:[43,45]

$$\Delta T/T = [\rho(Q)/\rho(F)]\Delta f/f$$

where T = total thickness of crystal and film, ΔT = change in thickness, $\rho(Q)$ = density of crystal (quartz), $\rho(F)$ = density of film, f = crystal resonant frequency, and Δf = crystal frequency shift. It has been shown that when the frequency shift is small, $\rho(Q)T/f$ is a constant.[43] The equation can then be simplified to:

$$\Delta T = [K/\rho(F)]\Delta f$$

where $K = \rho(Q)T/f$.

Since $\Delta T = [K/\rho(F)]\Delta f$,

then $\Delta T \cdot \rho(F) = K \cdot \Delta f$

and $\Delta T \cdot \rho(F) = \text{cm} \times \text{g/cm}^3 = \text{g/cm}^2 = \text{g/A}$

where g = grams and A = surface area

then $\Delta g/A = \Delta T\rho(F)$

and $\Delta g = A \cdot \Delta T \cdot \rho(F)$

$= A \cdot K \cdot \Delta f$

and $\Delta g = \frac{A \cdot \rho(Q) \cdot T \cdot \Delta f}{f}$

Using this final equation, we can calculate the grams of metal being deposited per hour onto the microbalance and thus onto our KBr window. The following is a model calculation for a calcium deposit. The microbalance frequency

was decreasing at a rate of 0.2405 Hz/hour. The thickness of the crystal and film was assumed to be very near that of the crystal alone in the beginning hours of the vaporization.

$$\Delta g = \frac{A \cdot \rho(Q) \cdot T \cdot \Delta f}{f}$$

$$\Delta g = \frac{(1.40\ cm^2)(2.5 g/cm^3)(0.028 cm)(0.2405 Hz/hr)}{(5881.38\ Hz)}$$

$$\Delta g = 4.0 \times 10^{-6} \text{ grams/hour}$$

$$\frac{4.0 \times 10^{-6}\ g/hr}{40.09\ g/mole} = 9.9 \times 10^{-8} \text{ moles/hr}$$

$$= 9.9 \times 10^{-5} \text{ mmoles/hr}$$

In our experimental design, the KBr window was 2 cm closer to the furnace effusion hole than the microbalance. By replacing this KBr window with a second microbalance, it was determined that the window accumulates three times the amount of metal than the first microbalance. Assuming that all the metal which hit the window was trapped, we calculated the actual amount of metal being deposited on the KBr window as being 3.0×10^{-4} mmoles/hr for calcium and 5.0×10^{-5} mmoles/hr for magnesium. During each experiment, the matrix gas flow was adjusted to 1.6 mmoles/hr. This resulted in a matrix gas/metal ratio of 5.3×10^3 for Ca and 3.2×10^4 for Mg. For each alkyl halide, the ratio of Ar to CH_3X was 152 to 1.

The magnesium (Alfa products 99.99%) and calcium were outgassed at elevated temperatures prior to depositions. Methyl iodide (Aldrich 99%), methyl bromide (Linde 99.5%), methyl chloride (Matheson 99.5%), and methyl fluoride (Matheson 99%) were frozen at liquid N_2 temperature and volatile impurities were pumped off. This degassing cycle was carried out several times for each gas. The methane (Linde 99%) was passed through degassed molecular sieves (13x) at 77°K to remove unwanted water and oxygen. The argon (Linde 99.99%)

was exposed to a copper catalyst (Chemical Dynamics R3-11) to scavenge any unwanted oxygen. Argon and each alkyl halide were mixed in a 3.5 liter gas bulb using convection heating. The dilution ratio of Ar to CH_3X was 152:1 in all cases.

Typical furnace temperatures were between 360° - 480°C for Mg and 460° - 560° for Ca. Total vaporization periods were about 12 hours. However, with the use of a shutter, which blocked the KBr window during spectroscopic observation and during periods of instrument adjustment, the actual vaporization time for the metal flux in contact with the KBr window was reduced to between one and three hours.

Spectroscopic measurements were made using a Cary 14 UV-Visible Spectrophotometer. A clean KBr window served as a reference sample. The slit width was automatically varied between 0.04 mm and 0.1 mm. Typically scans were made from 650 nm to 400 nm for Ca and from 400 nm to 240 nm for Mg. During each separate experiment, however, periodic scans were done from 650 nm to 240 nm in search of any new product or impurity peaks. The scan speed was set at 0.25 nm/sec. After an experiment was completed, the matrix appeared almost transparent with a light brown tint.

In each initial experiment, the matrix gas flow rate, the temperature of the matrix and the deposition rate of the metal were all systematically varied to achieve optimum isolation conditions. When these conditions were correct, absorptions due to M, M_2, and M_x were observed and growth rates of each species were recorded. Growth was monitored by determining the peak areas using an Apple Computer with Graphics Tablet software. UV-visible band assignments were made based on prior literature which was discussed earlier in this thesis.

Experimental Procedure

The experimental procedure followed for a typical M + CH_3X reaction is as follows: The rotary pump should be turned on several hours before the experiment is to begin. When the vacuum gauge reads 50 microns or below, the liquid N_2 trap should be filled and the diffusion pump should be turned on. The water valve for the diffusion pump should also be turned on at this time. It generally requires about one hour for the diffusion pump to sufficiently evacuate the entire matrix chamber. Both gate valves and the main disc sealed valve should be open during the entire pump down process. After one hour, the vacuum gauge should read about 5-10 microns. At this time the cold cathode gauge can be turned on to record an accurate background pressure inside the matrix chamber. When this pressure reads less than 4×10^{-5} torr, the water valves for the electrodes and the cryocooler should be opened. It is important to get a high water circulation rate through the cryocooler, therefore, this valve should be opened all the way. The next step is to turn on the cryocooler and commence cooling the KBr window. The Digital temperature indicator/controller should be set at the desired matrix temperature. It will generally take one hour to cool from room temperature down to 9K. During this cooling down cycle, the furnace should be turned on and slowly allowed to heat up to the vaporization temperature. The KBr window should be rotated 90° from the furnace so that the blind blocks any vaporizing metal from reaching the KBr window. When the furnace and KBr window have reached the desired temperatures, the actual experiment can begin. The microbalance and digital frequency counter should be turned on and the initial frequency recorded. The first step is to isolate the metal species in an Ar matrix. The valve on the Ar gas bulb should be opened and the needle valve will be used to control the amount of gas inlet into

the matrix chamber. The needle valve is typically opened until the pressure inside the matrix chamber indicates 900 microns, which is the pressure generated at the proper flow rate. At this time the KBr window should be rotated back 90° so the metal/Ar will begin depositing on it. The actual time of deposition should be measured with a stop watch. A reading of the microbalance should be taken at the beginning and the end of each deposition period. When the desired deposition time is complete, the window is again rotated 90° into the UV-visible source path for spectroscopic observation. Then the needle valve inleting the Ar is closed and the blind is once again blocking any further metal vapor from contacting the KBr window. A UV-visible spectrum is then recorded. This cycle is carried out several times until the metal species are being isolated and a growth rate for each species can be recorded.

When changing the matrix gas from Ar to Ar/CH_3X or vice-versa, the following adjustments are carried out. First the valve on the Ar gas bulb is closed. Then both gate valves are closed and any existing Ar in the apparatus is pumped away. Both gate valves are again opened and background pressure allowed to stabilize. The valve on the Ar/CH_3X gas bulb is then opened and the flow rate into the matrix chamber is controlled by the needle valve. The deposition procedure is then identical with that stated above.

When the deposition cycles are complete, an annealing experiment can be carried out by first closing the needle valve and any opened gas bulb valves. The window is then rotated into the spectroscopic observation path and the annealing temperature is then adjusted using the Digital temperature controller. When the annealing time is complete the KBr window is cooled back down to 9K and a spectrum is recorded.

When the experiment is completed, the shut down procedure begins by turning off the diffusion pump and isolating it from the rest of the system by closing the appropriate gate valve. Then the furnace as well as cryocooler can be shut off. The circulating water for the diffusion pump, electrodes, and cryocooler should be left on until the system is adequately cooled. It will take approximately six hours for the KBr window to warm to room temperature. At this time the window can be changed and another experiment can be carried out.

Results

Figures 2 and 3 show the typical spectra obtained upon codepositing Ca and Mg with Ar at 9K. The individual bands that were observed and their transitions are summarized in Table II. The relative intensities of each peak could change from matrix to matrix depending on particular reaction conditions. Some peaks appeared to be broader than the expected electronic absorptions observed by others, and we attribute this to the "matrix effect" where absorptions in nonequilibrium lattice sites tend to broaden a transition line. The fine and detailed structures of the dimers previously reported[27] were not needed in our work and therefore were not sought after. The intensity of the atom peaks were usually much weaker than that of the clusters. This was a result of our higher furnace and higher matrix temperatures, and the use of Ar as the matrix gas, allowing more diffusion and metal aggregation to occur. This was beneficial for our work since we were particularly interested in the reactivity of clusters.

TABLE II. UV-Visible Assignments for Matrix Isolated Magnesium and Calcium Species Observed in this Study.

Wavelength (nm)	Species	Assignment	Reference
265	Mg_2	$^1\pi_u \leftarrow {}^1\Sigma_g$	27,30
285	Mg	$^1P(3s3p) \leftarrow {}^1S(3s^2)$	23,27,33
291	Mg_x		
306	Mg_4		
318	Unknown		
344	Mg_3		
370	Mg_2	$A^1\Sigma_u^+(^1S+{}^1P) \leftarrow X^1\Sigma_g^+(^1S+{}^1S)$	23,30
374	Ca_2	$^1\pi_u \leftarrow {}^1\Sigma_g^+$	23
415	Ca	$4s4p\,{}^1P_1 \leftarrow 4s^2\,{}^1S_0$	20,21
448	Ca	$^1D_2 \leftarrow {}^1S_0$	20
470	Ca_x		
505	$Ca_x + Ca_2$		
550	Ca_x		
648	Ca_2	$^1\Sigma_u^+(^1S+{}^1P) \leftarrow {}^1\Sigma_g^+(^1S+{}^1S)$	27

Figure 2 shows the absorption spectrum of Ca codeposited with argon at 9K. The band assignments have been discussed earlier in this paper and will be reiterated here for clarity. The Ca atomic peak is seen as an asymmetric doublet centered at 415 nm. A second forbidden atomic transition is seen at 448 nm. This latter assignment is questionable due to its obvious intensity. Earlier reports[20,23] indicate this transition should only be about 4% of the size of the prior atomic transition. Our results have shown this transition to be between 15% - 45% of the size of the 410 nm doublet. It is possible that the source of the band is something other than Ca atoms. At the present time we will refer to this band as the $^1S - {}^1D$ Ca atomic transition, due to the lack of conclusive evidence stating otherwise. The largest peak at 470 nm is the Ca_x band, and is seen as a doublet. Another cluster peak shows up at 550 nm. Dimeric species appear at 374 nm and 505 nm. The latter wavelength has formerly been assigned as a combination of Ca_x and Ca_2.[20]

Figure 2. Visible absorption spectrum of calcium codeposited with argon at 9K.

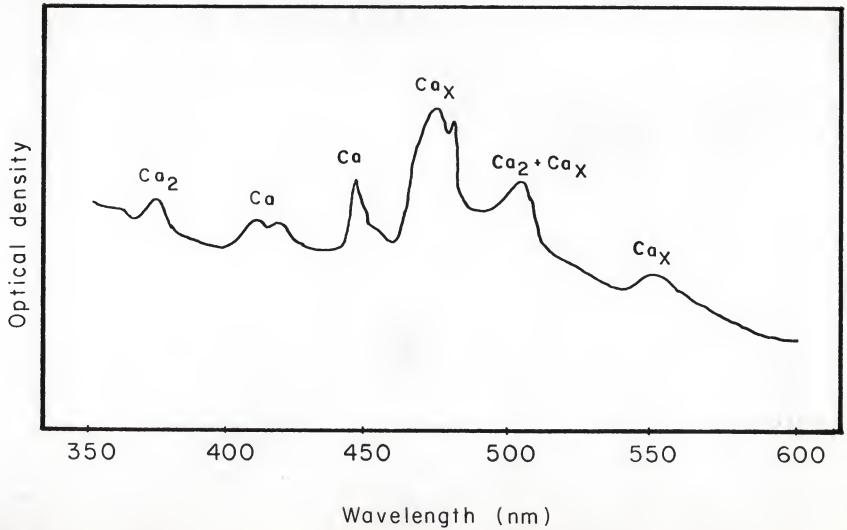
Optical density
Ca2
Ca
Ca
CaX
Ca2 + CaX
CaX
350
400
450
500
550
600
Wavelength (nm)

Figure 3 illustrates the absorption spectrum of Mg in an argon matrix at 9K. The only atomic transition is seen at 285 nm. Dimer bands show up at 370 nm and 265 nm. Both are broad peaks with medium intensity. The absorptions at 344 nm, 306 nm and 291 nm can be assigned to Mg_3, Mg_4 and Mg_x respectively.[23] Other transitions at 318 nm and 410 nm have previously been described as Ba and Ca impurities.[27] There is however, a Be atomic line that also has a transition in this same region (315-318 nm) and should not be ruled out as a possible impurity.

Figure 3. UV-visible absorption spectra of magnesium codeposited with argon at 9K.

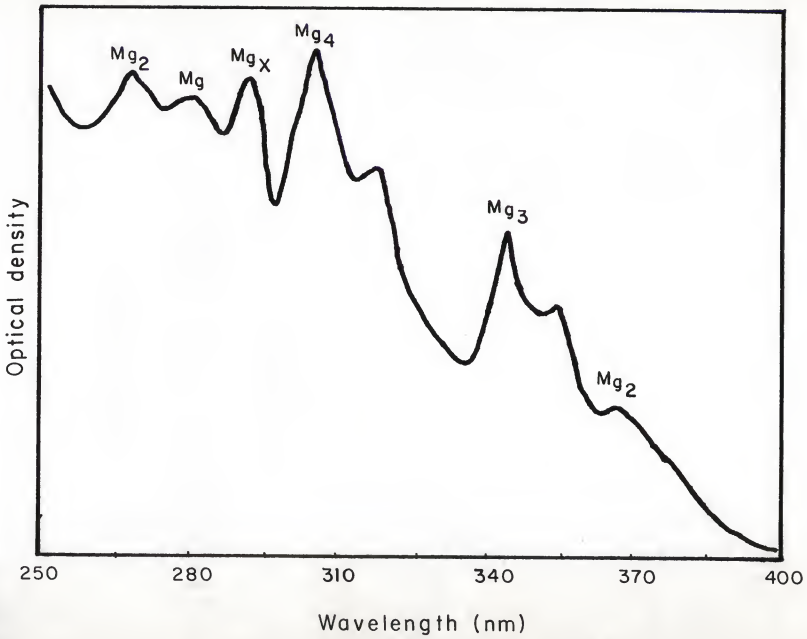
Mg2
Mg
MgX
Mg4
Mg3
Mg2
Optical density
250
280
310
340
370
400
Wavelength (nm)

Figures 4-15 illustrate the results of the metal species reacting with a particular alkyl halide. Each plot shows the absorption area vs. deposition time for the various metallic transitions observed. In all cases, the metal aggregates were allowed to build in a series of short deposits, with spectra taken after each deposit (this is seen as the first of five sections in the graph). Then the metal and alkyl halide were allowed to react and codeposit for another series of short deposits (section two in the graph). The third section of the graph again shows the growth rate of only the metal species. Then the fourth section indicates the resulting changes in area as metal and alkyl halide are further deposited in the presence of each other. During the entire deposition period, the metal was vaporizing at a constant rate. The breaks in the graph simply indicate a change in matrix gas from pure Ar to Ar/CH_3X. The last section shows the resulting absorptions after being annealed for 10 minutes at 25-35°K. Two different scales are needed (one on each side of the graph) due to the differences in absorption areas of each species. The arrows indicate which scale is used.

Ca + CH_3Cl. Inspection of figure 4 shows the differences in reactivity between the atom and cluster species. During the first section, all bands were growing at a constant rate. Upon switching from pure Ar to Ar/CH_3Cl, there is a dramatic increase in the growth rate of the atoms. The area under this atomic peak was enhanced 400% by a four minute addition of CH_3Cl. At the same time, however, the area under the bands Ca_x, Ca_2 and Ca (^1S - ^1D) actually leveled off or decreased slightly. With the second addition of pure Ar (third section), we observed consistent growth rates for all species. And in the presence of more Ar/CH_3Cl, we again observed tremendous growth for atoms and stabilization or decreases in all other species. The final section indicates the constant decreases observed for all species upon annealing.

Figure 4. Visible absorption area versus time for calcium atoms and clusters codeposited with methyl chloride.

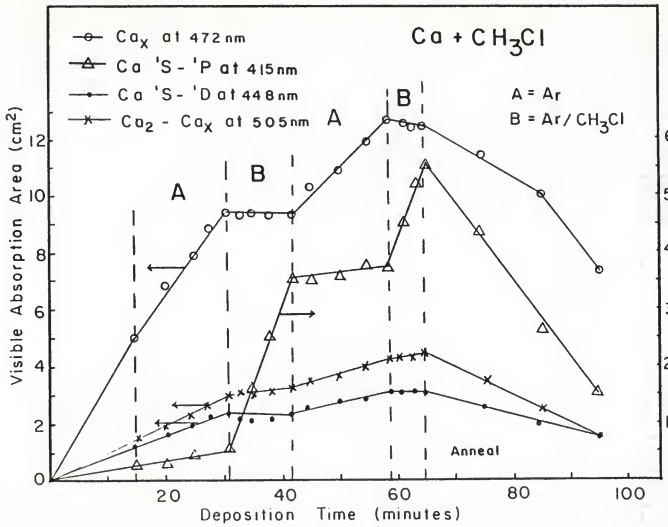
Ca_x at 472 nm
Ca $^1S - {}^1P$ at 415 nm
Ca $^1S - {}^1D$ at 448 nm
$Ca_2 - Ca_x$ at 505 nm
$Ca + CH_3Cl$
A = Ar
B = Ar/CH_3Cl
A
B
A
B
Anneal
Visible Absorption Area (cm^2)
Visible Absorption Area (cm^2)
Deposition Time (minutes)
0
2
4
6
8
10
12
10
20
30
40
50
60
20
40
60
80
100

Figure 5 shows individual isolation of the calcium atomic (415 nm) transition. This growth rate versus optical density plot demonstrates the enhancement in area observed in the presence of CH_3Cl. Similar plots were observed in other reactions where the atoms appeared nonreactive. No new bands were observed in the entire UV-visible region as a result of the CH_3Cl addition.

Figure 5. Visible spectrum of Ca atoms at 415 nm. The increase in intensity for the atomic transition is observed in the presence of Ar/CH_3Cl.

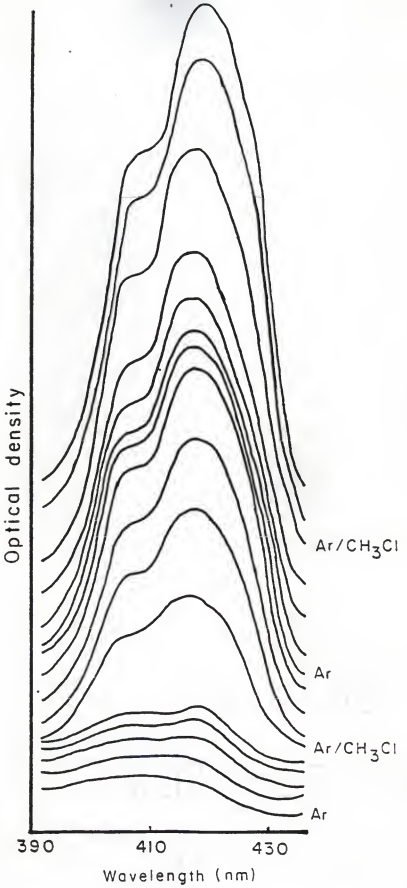
Optical density
Ar/CH3Cl
Ar
Ar/CH3Cl
Ar
390
410
430
Wavelength (nm)

Ca + CH_3Br. In figure 6 we see results virtually identical to the previous Ca + CH_3Cl case. Again it can be ascertained that atoms shown by Ca $^1S \rightarrow {}^1P$ transition are not reacting, and are therefore being produced or accumulated. The other calcium species seem to react with CH_3Br and decrease or stabilize in absorption area. The growth rate for the atomic transition in the presence of CH_3Br does not seem to be as great as it was in the presence of CH_3Cl. The area under the atomic peak ($^1S \rightarrow {}^1P$) increased about 200-300% for a three minute exposure to CH_3Br. The asymmetric doublet structure of this $^1S \rightarrow {}^1P$ transition presented itself in an interesting fashion in this experiment. The doublet is observed as a result of a vacancy being present next to a metal atom.[21] In the CH_3Cl experiment this doublet appeared as a strong absorption centered at 415 nm with a small shoulder at 410 nm. In the presence of CH_3Br, however, this absorption appeared with the small shoulder shifted to a higher wavelength. The center of this atomic transition remained at 415 nm, but the shoulder appeared at 422 nm. The wavelength shift of this shoulder is presumably caused by the alkyl halide entering into the solvent cage at a non-equilibrium site. The two halides appear to perturb this solvent cage in a slightly different fashion, and thus we see the shoulder shifting wavelengths from one side of the atomic transition to the other. No new product peaks were observed in this experiment, and all existing transitions decreased rapidly upon annealing.

Figure 6. Visible absorption area versus time for calcium atoms and clusters codeposited with methyl bromide.

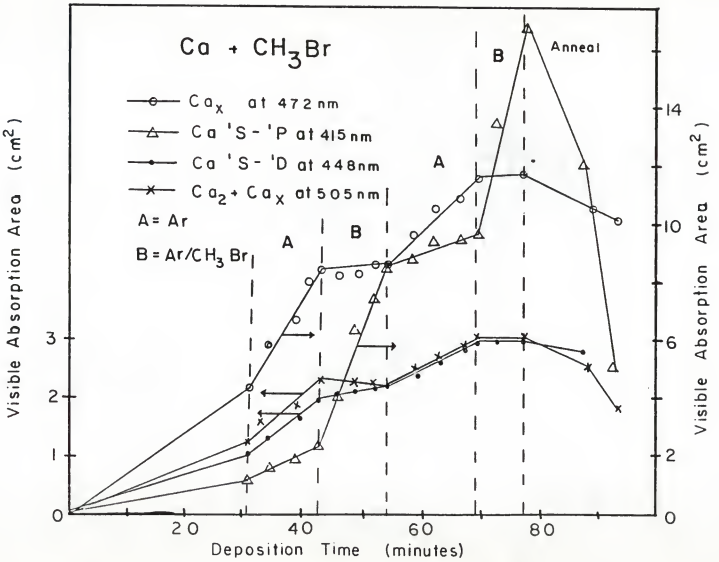
Ca + CH3Br
Cax at 472 nm
Ca 1S - 1P at 415nm
Ca 1S - 1D at 448nm
Ca2 + Cax at 505nm
A = Ar
B = Ar/CH3 Br
A
B
A
B
Anneal
Visible Absorption Area (cm2)
Visible Absorption Area (cm2)
Deposition Time (minutes)
0
1
2
3
0
2
6
10
14
20
40
60
80

Ca + CH_3F. Figure 7 shows the results of calcium reacting with CH_3F at 9K. These results are unique for two reasons. First, it is the only experiment where new product peaks were observed as a result of the addition of the methyl halide. In this case, two new absorptions were observed at 492 nm and 458 nm. These peaks were very dependent upon the CH_3F concentration and increased very sharply in the presence of CH_3F, and likewise decreased very rapidly in the absence of CH_3F. The second unique feature observed in this plot is a reactivity not previously seen before by the metal species. In this case, the cluster, dimer, and atom ($^1S \rightarrow {}^1P$) all appear to react with the methyl fluoride and show decreases in absorption areas in the presence of the matrix gas. It is the questionable atomic transition at 445 nm that indicates no reactivity and thus increases with addition of CH_3F. This is the first example where this peak does not mimic the metal clusters and instead shows individual inertness. These results can be misleading and should be explained further. The new product peaks observed overlapped with existing transitions and made integration of the primary calcium species very difficult. The growth of the product peaks was very erratic upon changing the matrix gas and resulted in a shift of the baseline. This shift caused existing peaks to increase or decrease in absorption area and made it appear as if the atoms and clusters were reacting very rapidly in the presence of CH_3F. To compensate for the moving baseline, integrations were also made using an estimated baseline which would have resulted if the product peaks had not been observed. These integrations were then compared with those actually obtained. From these results, it still appears that the Ca atoms, dimers, and clusters were reacting with the CH_3F, however, not quite as readily as it might appear in Figure 7. The Ca $^1S \rightarrow {}^1D$ transition cannot be accurately described as representing a species that is reacting or not reacting since

it was involved in significant overlap. The intensity of this peak increased upon addition of CH_3F, but we believe much of this increase was caused by the band overlap of the product peak centered at 458 nm. The annealing process for this reaction showed all species, including the two product peaks, decreasing at similar rates.

Figure 7. Visible absorption area versus time for calcium atoms and clusters codeposited with methylfluoride at 9K.

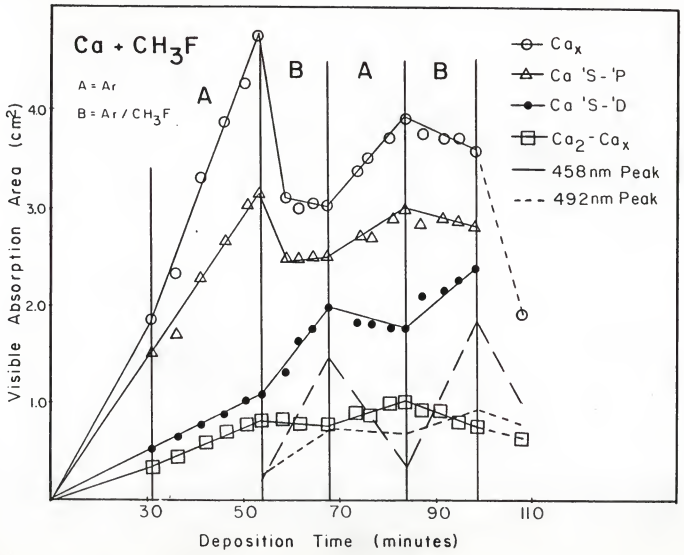

Visible Absorption Area (cm2)

Ca + CH_3I. It is well known that CH_3I reacts very rapidly to form Grignard reagents. Figure 8 reinforces this notion by illustrating the immense reactivity of the calcium species with CH_3I. Ca, Ca_2, and Ca_x all appear to react in an equivalent fashion. This is the only example in our study of calcium and magnesium where all the isolated species showed definite reactivity with the alkyl halide.

Figure 8. Visible absorption area versus time for calcium atoms and clusters codeposited with methyliodide at 9K.

Ca + CH3I
A = Ar
B = Ar/CH3I
Cax at 472 nm
Ca 1S - 1P at 415 nm
Ca 1S - 1D at 448 nm
Ca2 + Cax at 505 nm
Visible Absorption Area (cm2)
Deposition Time (minutes)
0
20
40
60
80
2
4
6
8
A
B

Ca + CH_4. In these observations we observed entirely the opposite results of the previous study. CH_4 appeared to be inert toward any of the calcium species. Figure 9 shows a constant growth in absorption areas until the inlet of Ar/CH_4. At this point the slopes in the plot all decrease slightly, but again growth is at a constant rate and is maintained at this rate for the duration of the experiment. The second time the matrix gas was changed from Ar to Ar/CH_4, we observed no change in the growth rates of any of the isolated species indicating no reaction was occurring with methane. At the end of the experiment pure CH_4 was inlet for five minutes. Again the calcium species maintained the same growth pattern in their absorption areas, indicating no formal reaction was occurring. When this experiment was complete, CH_3F was inlet for eight minutes and allowed to react with the calcium. This reaction produced excellent isolation of the existing calcium absorptions as well as the two product peaks. The resulting data obtained, simply reinforced our earlier discussion of Ca + CH_3F.

Figure 9. Visible absorption area versus time for calcium atoms and clusters codeposited with methane at 9K.

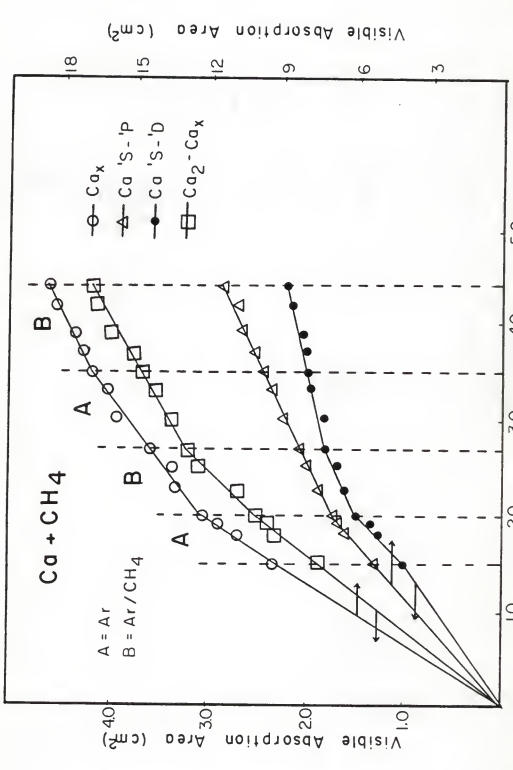
Ca + CH4
A = Ar
B = Ar/CH4
A
B
A
B
Ca x
Ca 1S - 1P
Ca 1S - 1D
Ca2 - Cax
Visible Absorption Area (cm2)
Deposition Time (minutes)
10
20
30
40
50
10
20
30
40
3
6
9
12
15
18

Mg + CH_4. Figure 10 shows the analogous experiment with magnesium co-deposited with argon at 9K. The results are much the same as in the calcium case. CH_4 does not react with any of the species isolated. The slopes of the absorption areas remain constant upon addition of CH_4 and do not change when the matrix gas is changed to pure CH_4, pure argon, or a 1:150 mixture of the two.

Figure 10. UV-visible absorption area versus time for magnesium atoms and clusters codeposited with methane at 9K.

Mg + CH4
Mg at 285nm
Mg2 at 370nm
Mg2 at 265 nm
Mg3 at 344 nm
A = Ar
B = Ar/CH4
A
B
A
B
UV-Visible Absorption Area (cm²)
2.5
2.0
1.5
1.0
.5
20
30
40
47
Deposition Time (minutes)
UV-Visible Absorption Area (cm²)

Mg + CH_3Br. Our initial experiments with Mg + CH_3Br have been thoroughly explained in an earlier study.[37] Figure 11 summarizes the results obtained. The reactivity of Mg + CH_3Br is very similar to that of Ca + CH_3Br. In both cases the atoms did not react, and were produced at a tremendous rate in the presence of methyl bromide. The higher aggregate species, however, did react and the absorption areas for these species decreased slightly. This study and the CH_4 study are the only two in which Ca and Mg behave identically. All other experiments showed a difference in one or more of the metallic species toward a particular methyl halide.

Figure 11. UV-visible absorption area versus time for magnesium atoms and clusters codeposited with methyl bromide at 9K.

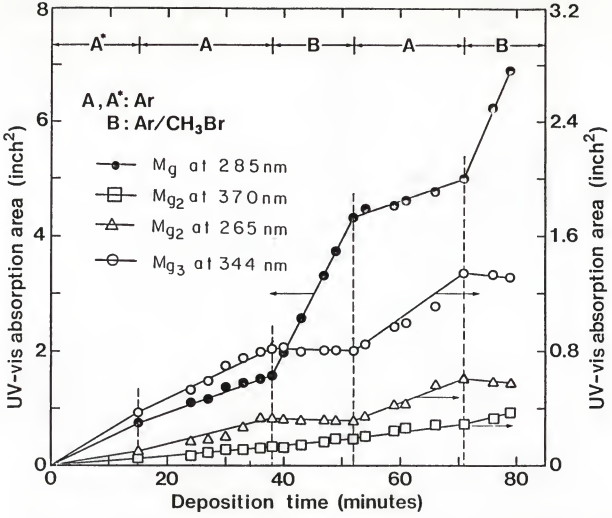
A*
A
B
A
B
A, A*: Ar
B: Ar/CH3Br
Mg at 285nm
Mg2 at 370nm
Mg2 at 265 nm
Mg3 at 344 nm
UV-vis absorption area (inch2)
UV-vis absorption area (inch2)
Deposition time (minutes)
0
2
4
6
8
0
0.8
1.6
2.4
3.2
0
20
40
60
80

Mg + CH_3I. Figure 12 shows unexpectedly that the magnesium atoms did not react with methyl iodide. Mg_2, Mg_3, and Mg_4 all showed definite reactions occurring in the presence of CH_3I. It appears that the larger clusters may be more reactive than smaller clusters. This observation is based on this experiment and calcium experiments where the slope due to the higher clusters decreased more rapidly than the corresponding smaller clusters. Upon annealing, a normal decrease in absorption areas was observed for all the species except Mg_2. The dimer actually increased in area indicating the diffusion of atoms into dimeric species upon warming. The cluttered appearance of the graph points out that most of the species were isolated to the same extant. The paralled growth rates demonstrates the equal reactivity of these species.

Figure 12. UV-visible absorption area versus time for magnesium atoms and clusters codeposited with methyl iodide at 9K.

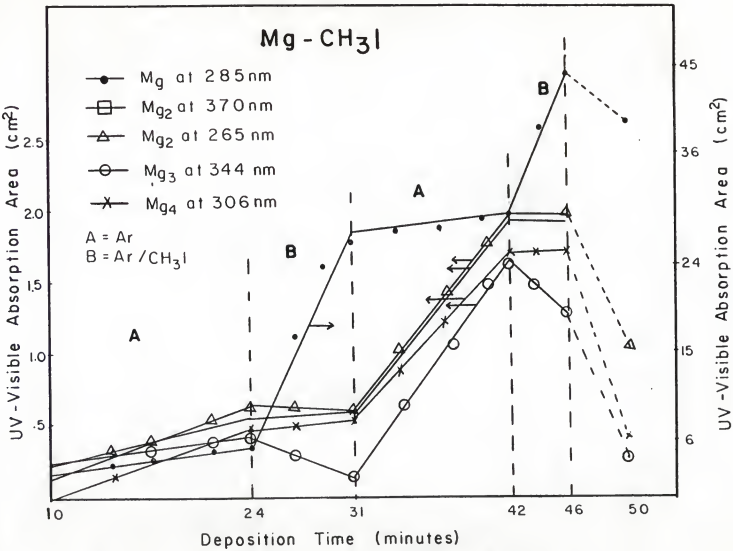
Mg - CH3I
Mg at 285nm
Mg2 at 370nm
Mg2 at 265 nm
Mg3 at 344 nm
Mg4 at 306nm
A = Ar
B = Ar / CH3I
A
B
A
B
UV - Visible Absorption Area (cm2)
UV - Visible Absorption Area (cm2)
Deposition Time (minutes)
10
24
31
42
46
50
.5
1.0
1.5
2.0
2.5
6
15
24
36
45

Mg + CH_3Cl. Magnesium codeposited with methyl chloride at 9K showed no reactivity with any of the metal species. In figure 13 we have combined all the higher aggregate Mg species into one category and labeled it Mg clusters. This is to avoid direct overlap of the absorption areas of the variable size metal clusters in the plot. The atoms and cluster species represented in this plot increased their absorption areas in the presence of CH_3Cl indicating no reaction occurred under these experimental conditions. Previous IR experiments have indicated that a product did indeed form in the reaction of Mg + CH_3Cl.[35] This report does however stress the weakness of the product peaks observed, compared to other magnesium + alkyl reactions. The lack of reactivity observed in our experiments could be a result of the difference in concentrations used. The IR study reportedly was carried out at much higher concentrations. They employed a gas to metal ratio between 100/1 and 1000/1. Our reaction was studied under much more dilute conditions. These conditions were necessary to maintain a uniformity with other reactions which showed extreme reactivity under these conditions.

Figure 13. UV-visible absorption area versus time for magnesium atoms and clusters codeposited with methyl chloride at 9K.

Mg + CH3Cl
Mg atoms
Mg clusters
A = Ar
B = Ar/CH3Cl
A
B
A
B
UV - Visible Absorption Area (cm2)
Deposition Time (minutes)
10
20
30
40
46
.5
1.0
1.5
2.0
2.5
6
12
18

Mg + CH_3F. This experiment again demonstrated the greater reactivity of the larger clusters. Mg_x and Mg_4 appeared to react while Mg_2 and Mg_3 did not. In general, our results have illustrated that small clusters mimic the larger cluster species. In this case however, we see reactivity only toward clusters (Mg_x), with x greater than three. First glance at figure 14, indicates Mg atoms have reacted in the same manner as the clusters. This is deceiving since they are reported using two different scales (left and right in figure 14). In actuality, the atomic absorption area changes very little throughout the course of the experiment. The increases and decreases in this area only ranges about 0.2 cm^2, which is very close to the experimental error in our investigations. Therefore, it is not obvious whether the Mg atoms reacted or not. Since the growth rate changed very little, it implies very little, if any, reaction occurred. The atomic absorption did increase significantly upon annealing at 30K for ten minutes. This may imply that atoms are being produced due to a specific cluster size needed for optimum reactivity. All other metal species decreased consistently upon annealing.

Figure 14. UV-visible absorption area versus time for magnesium atoms and clusters codeposited with methylfluoride at 9K.

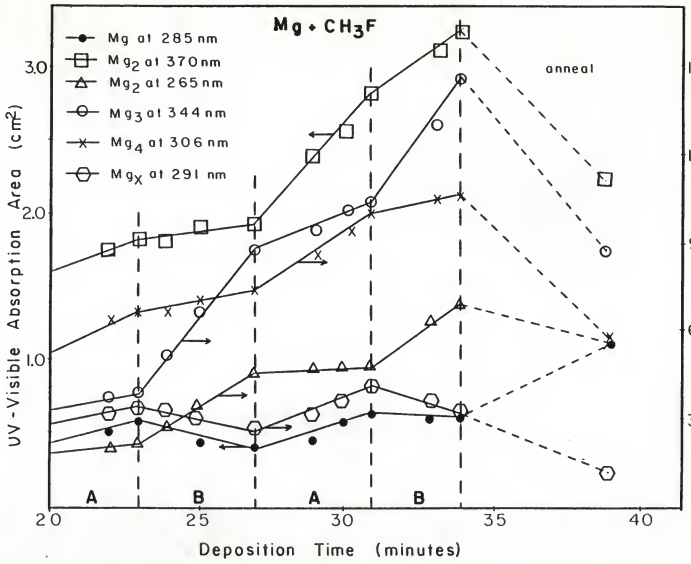
Mg + CH3F
Mg at 285 nm
Mg2 at 370 nm
Mg2 at 265 nm
Mg3 at 344 nm
Mg4 at 306 nm
MgX at 291 nm
anneal
A
B
A
B
UV - Visible Absorption Area (cm2)
UV - Visible Absorption Area (cm2)
Deposition Time (minutes)
3.0
2.0
1.0
15
12
9
6
3
20
25
30
35
40

Discussion

The results of our calcium and magnesium studies are presented in Tables III and IV. For each metal, the main species are shown. The results have been generalized into two categories, reacted and not reacted. An X indicates the species was not observed in that study, and a question mark implies the transition was weak and could not be integrated with accuracy.

The Anomalous Ca Peak

The first thing that should be discussed is our tenative assignment of the Ca $^1S \rightarrow {}^1D$ transition at 448 nm (see Figure 2). According to literature this transition is a forbidden transition that disobeys both the multiplicity and the angular momentum selection rules. It occurs as a result of lowering the symmetry so that ^1P and ^1D have a common irreducible representation which can mix to give observable intensity to this forbidden transition.[20] Both atomic transitions have two matrix sites, and in each site, there is observable intensity from both the $^1S \rightarrow {}^1P$ and $^1S \rightarrow {}^1D$ transitions.[23] This latter transition is expected to be between 4-6% of that seen for the $^1S \rightarrow {}^1P$. The band we see maintains at about 15-45% of this transition before alkyl halide is inlet. In the presence of the alkyl halide, this peak in no way resembles the $^1S \rightarrow {}^1P$ atomic transition. In fact we see better correspondence between this questionable peak and the cluster species than we do between it and the atomic transition. In the CH_3Br and CH_3Cl studies, we most definitely see an increase in the Ca atom concentration. At the same time, the peak in question mimics the cluster peaks and behaves the same way by losing absorption area. In the methyl fluoride case, Ca atoms, dimers, and clusters all seem to react while this transition appears to show no behavior that would indicate reactivity. In lieu of this evidence, we conclude that the transition observed at 448 nm is not due to the reported $^1S_0 \rightarrow {}^1D_2$

calcium atomic transition. This is not to say this transition does not exist in matrix isolation studies, but rather, that in our study this transition is buried in the noise and is simply not seen. Due to the close resemblance in behavior of this peak and cluster peaks, we attribute this transition to a cluster species. The reaction at Ca with CH_3F was the only example where the peak in question did not show identical reactivity with clusters. This was explained due to the band overlap occurring between this transition and a new product peak. The electronic transition as well as the size of the cluster responsible for this peak is unknown. The possibility of this transition being caused from an impurity is unlikely but is not being totally excluded. To summarize, the fact that this transition persisted after partial evaporation of the metal, and that identical behavior was observed between this peak and those for calcium clusters, leads one to logically conclude that the source of this transition is due to calcium clusters and not atoms.

Kinetic Considerations

Our results consistently demonstrate that metal clusters are more reactive than atoms under matrix isolation conditions. To explain this, we must first examine the formation of these clusters. Two acceptible modes of formation are possible.[46] A statistical formation would produce clusters as a result of the random placement of the atoms in a crystalline matrix. A kinetic explanation of formation states that clusters form during a very short period of time after condensation, while the metal atoms and the noble gas particles are still mobile. The kinetic explanation is the most reasonable based on the fact that when the matrix temperature is decreased from 9K to 6K, the atomic transitions increase in area while the cluster transitions decrease, presumably due to the lack of diffusion of metal atoms and

particles at the colder temperature. Kinetics can also help us to understand the differences in reactivity between the atoms and higher aggregates. Using a steady state analysis, we can explain the enhanced atom isolation in the presence of an alkyl halide. In general, dimers appear to mimic higher clusters and react in the same fashion. We suggest that it is the dimeric metal species which is reacting with the alkyl halide very rapidly. This reaction is so rapid that the dimer does not exist long enough to combine with other metal atoms to form higher aggregate species.

$$M + M_2 \xrightarrow{X} M_3 \quad \text{in the presence of } CH_3X$$

In this way, the dimers being produced by the collision of atoms are being used up and thus we see a stabilization or decrease in their absorption areas. At this same time, since it takes a dimer plus an atom (or another dimer) to produce a cluster, we also see a decrease in the growth rate for the M_x species. Since the dimers are reacting so rapidly, free atoms have no chance to combine with them to form higher aggregates, and thus we see an increase in the atom concentration at a continuous metal atom flux. This argument assumes that metal atoms do not react with the cluster Grignard product.

$$M + CH_3MMX \xrightarrow{X} CH_3M_3X$$

Figure 15 illustrates a reaction diagram for $M + CH_3X$. In this diagram the cluster Grignard product is shown to be about 8 kcal/mole more stable than the atom Grignard. The activated complexes are only proposed and have not been experimentally verified. The activated complex for the cluster Grignard may be stabilized by a four centered transition state. This transition state would allow a better orbital overlap between the dimer and the alkyl halide which would lower the activation energy. The corresponding three centered transition state of the atom Grignard would result in a higher activation energy. To extend the idea that cluster Grignards are more stable

than atom Grignards, we must look at the thermodynamics involved.

Figure 15. Reaction coordinate versus energy diagram for atom and cluster Grignard species.

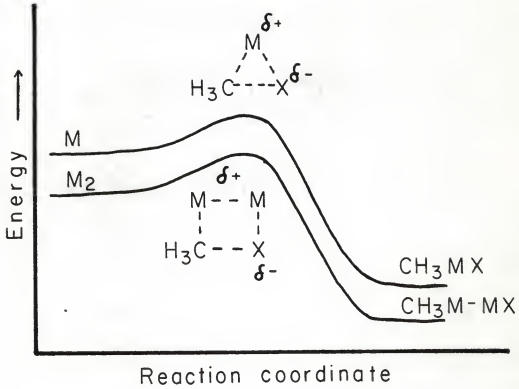
δ+
M
H3C
X
δ-
M
M2
δ+
M
M
H3C
X
δ-
CH3MX
CH3M-MX
Energy
Reaction coordinate

Thermodynamic Considerations

The fact that clusters react while atoms do not may be the result of more favorable reaction energetics. It has been demonstrated by Dykstra,[38] that the Mg-Mg bond is very weak in Mg_2 but is much stronger in the R-Mg-Mg-X species. This is an added driving force for the reaction, since three bonds are formed while only one bond is broken.

1.) $CH_3\text{-}X + M \longrightarrow CH_3\text{-}M\text{-}X$ Two bonds formed

2.) $CH_3\text{-}X + M\text{--}M \longrightarrow CH_3\text{-}M\text{-}M\text{-}X$ Three bonds formed
weakly bound

Additionally, the activation energy for reaction 2 may be lower due to a more facile electron transfer from M_2 than M. This may be the first step in the reaction:

$$\underset{\text{weakly bound}}{M\text{-}M} + CH_3X \longrightarrow \underset{\text{strongly bound}}{M\text{-}M^+}\ CH_3X^-$$

If this electron transfer step occurs first, then the reaction will rely heavily on the ionization potential of the metal. Metal clusters have been shown to have lower ionization potentials than atoms, resulting in a strongly bonded M_2^+ species.[47] This stability arises from the removal of an antibonding electron which results in a bond order of one-half for the diatomic species.[48] Porter,[48] reports an I.P. of 7.6 eV for Mg atoms, while the corresponding dimer has an I.P. of 6.7 eV. Also the Mg-Mg bond strength is 1.2 kcal/mole, while the ionized $Mg\text{-}Mg^+$ has a bond strength of 23.4 kcal/mole. This data reinforces our earlier postulate in that the dimer will be ionized easier than the atom which will result in a stronger M-M bond. The electron transfer will then be facilitated by the M_2^+ species resulting in a lower activation energy for the formation of the cluster Grignard.

$$M_2 + CH_3X \longrightarrow M_2^+CH_3X^- \longrightarrow CH_3M_2X$$

Also, as mentioned earlier, another reason M_2 or higher clusters are more reactive than atoms may be due to a favorable four centered transition state as seen in figure 15. The exothermicity of the overall reaction will depend on good ion pairing energy, low ionization potential for the metal particle, and a stronger M-M bond in the M_2^+ species.

Our results indicate that calcium may be more reactive than magnesium in forming cluster Grignards. The summarization of the results presented in Tables III and IV shows definite reactivity of Ca_2 and Ca_x with CH_3Cl and CH_3F. In the latter case two new product bands were observed. The corresponding reactions with Mg showed no reactivity of CH_3Cl with any magnesium species, and only slight Mg_x reactivity with CH_3F. Mg, Mg_2, Mg_3 and Mg_4 did not appear to react with CH_3F. These results can be partially explained by the lower ionization potential of calcium which would require less energy for the Ca_2^+ dimer to initiate the electron transfer process. The ion pairing energies would be expected to be similar for both calcium and magnesium; however, due to the larger radius of calcium atoms, this energy may be slightly less. To explain further why metal species would react with some alkyl halides but not with others, we need to examine the relative energies of the bonds involved.

Table III. A Summary of the Reactivities of Magnesium Codeposited With the Alkyl Halides.

	Magnesium Species					
Alkyl halide	Mg	Mg_2	Mg_3	Mg_4	Mg_x	Other
CH_3I	No	Yes	Yes	Yes	Yes	None
CH_3Br	No	Yes	Yes	X	Yes	None
CH_3Cl	No	No	?	No	No	None
CH_3F	No	No	No	Yes	Yes	None
CH_4	No	No	No	?	?	None

Yes - reaction was observed

No = reaction was not observed

X = species was not observed in this study

? = transition was weak and reactivity is not definite

Table IV. A summary of the reactivities of calcium codeposited with the alkyl halides.

Alkyl halide	Calcium Species				
	$Ca(^1S \rightarrow ^1P)$	$Ca(^1S \rightarrow ^1D)^a$	Ca_x	Ca_2	Other
CH_3I	Yes	Yes	Yes	Yes	None
CH_3Br	No	Yes	Yes	Yes	None
CH_3Cl	No	Yes	Yes	Yes	None
CH_3F	Yes	?	Yes	Yes	Two new peaks
CH_4	No	No	No	No	None

Yes = reaction was observed

No = reaction was not observed

? = reactivity is uncertain

a = tenative assignment based on literature values.

Bond Strengths

The fact that clusters were observed to react in some cases but not in others is interesting. Referring back to Tables III and IV we can examine the ambiguities observed in our study. The cases where clusters showed no reactivity were, Mg + CH_3Cl, CH_3F, CH_4 and Ca + CH_4. These four exceptions must have something in common. Table V indicates the bond strengths of the atomic species used in our experiments.[49] In all the examples (except Ca + CH_3F) where the metal clusters showed reactivity toward the alkyl halide, the bond strength for the metal-halogen bond is equal to or greater than that for the carbon-halogen bond. Even in the Ca + CH_3F study, there is only a two kcal/mole discrepancy. This can be totally alleviated when the recorded accuracy is taken into account. The four examples which showed no reactivity under our experimental conditions have metal-halogen bond strengths which are much less than the corresponding carbon-halogen bond strength. This appears to be the common link explaining reactivities of the examples studied. These data indicate that the reaction process can only be initiated if there is enough stabilization energy in the produced carbon-metal bond, metal-metal bond, and metal-halogen bond to overcome the cleavage of the carbon-halogen bond in the reactant. In this case, the metal-halogen bond strength is the most important. The metal-metal bond will be relatively weak and will only provide additional stabilization over the corresponding single metal atom CH_3MX species.

Table V. Bond strengths of diatomic species.

Dimeric Species	Bond strength kcal/mole
Ca-Br	76.6 ± 5.5
C-Br	67 ± 5
Mg-Br	71 ± 15
Ca-Cl	95 ± 3
C-Cl	95 ± 7
Mg-Cl	76 ± 3
Ca-F	126 ± 5
C-F	128 ± 5
Mg-F	110 ± 1.2
Ca-I	68 ± 15
C-I	50 ± 5
Mg-I	68
Ca-H	40.1
C-H	80.6 ± 0.2
Mg-H	47 ± 12

The bond strength argument can be used to explain the reactivity of most of the alkyl halides toward calcium and magnesium, but more explanation is needed to elucidate the CH_3F case. In the reaction Ca + CH_3F, the Ca-F bond strength is slightly less than that for C-F.[49] Even though the bond strength is less, we still observed a reaction occurring between Ca atoms, dimers and clusters with the CH_3F. Also the two new product peaks appearing indicate a type of bonding not previously seen in the alkyl-metal-halide complex. This bonding allows the electrons from the metal to be in a slightly different environment and thus we see a shift in the absorption wavelength. One possible explanation of this bonding may involve the interaction between the metal halide complex and the lattice structure of the solvent cage.

The crystal structure of frozen argon has been described as being a face-centered cubic structure.[50] In this structure there are three possible sites available to accommodate the metal species. The diameters of these sites have been described by Moskovits and Ozin.[51] They are, a tetrahedral hole (diameter 0.85 Å), an octahedral hole (diameter 1.56 Å), and a substitutional hole (diameter 3.75 Å). The first two would already exist in the frozen argon lattice and the latter would be formed when a host atom is removed and the metal atom is substituted for it.[51] The magnesium and calcium atoms would be located in the substitutional holes for our experiments since the octahedral and tetrahedral holes are too small. In the Ca + CH_3F reaction however, it would be possible for a fluorine atom to fit into an octahedral site. If the fluorine atom is in this site, it may form a complex with a Ca atom which is already frozen. This unique type of complexation may be of the type:

$$CH_3F \text{ --- } Ca \text{ or } F\text{-}CH_3 \text{ --- } Ca$$

Bonding of this type would be different than that previously explained and

could account for the presence of the two new peaks observed in the Ca + CH_3F reaction. Fluorine is the only halide which could fit into an octahedral site, and CH_3F is the only alkyl halide studied which resulted in new transitions when codeposited with Ca or Mg. The fact that these complexed calcium peaks developed and increased in intensity very dramatically when the matrix gas was changed from Ar to Ar/CH_3F, indicates that it is the halide which is responsible for the existence of these bands. This type of complexation would be secondary and we would still expect Ca clusters to bind by the $H_3C\text{--}Ca_2\text{-}F$ formation mode.

Conclusion

This study of the reactions of calcium and magnesium atoms and clusters with alkyl halides has produced considerable evidence that metal clusters are the more reactive species when forming Grignard type compounds under matrix isolation conditions. In most experiments, the clusters reacted while the atoms did not. We propose an electron transfer mechanism which is made possible by the lower ionization potential of the clusters. The corresponding cluster Grignard formed has been shown by theoretical calculations to be more thermodynamically stable than the atom Grignard.[38] The following results are a summarization of reactions we observed in our study of calcium and magnesium codeposited with methyl halides and methane.

$$Ca + CH_3X \longrightarrow CH_3CaX \text{ or } CH_3X\text{---}Ca \quad Ca\text{---}CH_3X$$
where X = I,F

$$Ca_2 + CH_3X \longrightarrow CH_3Ca_2X$$
where X = I,Br,Cl,F

$$Ca_x + CH_3X \longrightarrow CH_3(Ca)_xX$$
where X = I,Br,Cl,F

$$\text{Any Ca species} + CH_4 \longrightarrow \text{No Rxn}$$

$$Mg + CH_3X \not\longrightarrow CH_3MgX \quad \text{for any X}$$

$$Mg_2 + CH_3X \longrightarrow CH_3Mg_2X$$
$$X = I,Br$$

$$Mg_3 + CH_3X \longrightarrow CH_3Mg_3X$$
$$X = I,Br$$

$$Mg_4 + CH_3X \longrightarrow CH_3Mg_4X$$
$$X = I$$

$$Mg_x + CH_3X \longrightarrow CH_3(Mg)_xX$$
$$X = I,Br,F$$

$$\text{Any Mg species} + CH_4 \longrightarrow \text{no RXN}$$

The results of this work have great implications on understanding how Grignard reagents are formed from bulk magnesium. Whitesides and coworkers,[52] have considered several possible transition states in the mechanistic formation of Grignard reagents. These possibilities have been narrowed down with the aid of kinetic studies, but the actual mechanism of formation is still not clearly understood. It may be possible that CH_3Mg_2X type species are formed in a regular RMgX Grignard preparation. However, evidence by Dykstra[38] indicates that addition of a second alkyl halide to the dimagnesium Grignard would produce two simple Grignards.

$$RX + RMg_2X \longrightarrow 2RMgX$$

Therefore it is hard to detect the presence of dimagnesium species in a normal Grignard reaction. It may be possible to prepare CH_3Mg_2X on a large scale under the right experimental conditions. We are currently trying to prepare such species in our laboratory.

References

1.) I. Norman, and G. Porter, Nature, 174, 508 (1954); E. Whittle, D. A. Dows, and G. C. Pimentel, J. Chem. Phys., 22, 1943 (1954).

2.) E. D. Becker, and G. C. Pimentel, J. Chem. Phys., 25, 224 (1956).

3.) Milton J. Linevsky, J. Chem. Phys., 34, 587 (1961).

4.) H. E. Hallam, "Vibrational Spectroscopy of trapped Species", J. Wiley, London (1973).

5.) J. M. Bassler, P. L. Timms, and J. L. Margrave, Inorg. Chem., 5, 729 (1966).

6.) P. L. Timms, J. Amer. Chem. Soc., 89, 1629 (1967); P. L. Timms, Inorg. Chem., 7, 387 (1968).

7.) P. S. Skell, and J. J. Havel, J. Amer. Chem. Soc., 93, 6687 (1971).

8.) L. Andrews, and G. C. Pimental, J. Chem. Phys., 44, 2361 (1966).

9.) L. Andrews, J. Chem. Phys., 48, 972 (1968).

10.) L. Andrews, J. Chem. Phys., 50, 4288 (1969).

11.) R. L. Dekock, Inorg. Chem., 10, 1205 (1971).

12.) J. K. Burdett and J. J. Turner, Chem. Commun., 885 (1971).

13.) Geoffrey A. Ozin and Martin Moskovits, "Cryochemistry", J. Wiley & Sons, New York, (1976) pg. 1.

14.) G. T. Reedy, S. Bourne, and P. T. Cunningham, Analytical Chemistry, 51, 1535 (1979).

15.) A. J. Barnes, W. J. Orville-Thomas, A. Mübber, and R. Gaufres "Matrix Isolation Spectroscopy" Vol. 76, D. Reidel Publishing Co. London, (1980) pg. 531.

16.) J. S. Shirk and H. H. Classsen, J. Chem. Phys., 54, 3237 (1971).

17.) H. Huber, G. A. Ozin, and A. Vander Voet, Nature, 232 166, (1971); G. A. Ozin & A. Vander Voet, J. Chem. Phys., 56, 4768 (1972).

18.) T. K. McNab & P. H. Barrett, in I. J. Graverman (Ed.), Mössbauer Effect Methodology, Vol. 7, Plenum, New York, (1971).

19.) A. Thompson, paper presented at the "Meldola Lecture Symposium." University College, London, (1974).

20.) L. Andrews, W. W. Duley, and L. Brewer, J. Mol. Spec., 70, 41 (1978).

21.) J. E. Francis, Jr., and S. E. Webber, J. Chem. Phys., 56, 5879 (1972).

22.) L. Brewer and J. L. F. Wang, J. Chem. Phys., 56, 4305 (1972).

23.) J. C. Miller, R. L. Mowery, E. R. Krausz, S. M. Jacobs, H. W. Kim, P. N. Schatz, and L. Andrews, J. Chem. Phys., 74, 6349 (1981).

24.) V. E. Bondybey, J. Chem. Phys., 68, 1308 (1978).

25.) H. J. Balfour, and R. F. Whitlock, Chem. Comm., 1231 (1971).

26.) J. C. Miller, and L. Andrews, Chem. Phys. Letters, 50, 315 (1977).

27.) J. C. Miller, B. S. Ault, and L. Andrews, J. Chem. Phys., 67, 2478 (1977).

28.) D. Schnepp, J. Phys. Chem. Solids, 17, 188 (1961).

29.) L. Brewer and J. L. F. Wang, J. Mol. Spec., 40, 95 (1971).

30.) L. B. Knight and M. A. Ebener, J. Mol. Spec., 61, 412 (1976).

31.) L. Andrews and G. C. Pimentel, J. Chem. Phys., 47, 2905 (1967); R. B. Merrithew, G. V. Marusak, and C. E. Blount, J. Mol. Spec. 29, 54 (1969).

32.) W. W. Duley and J. Ryan, Chem. Phys. Lett., 21, 208 (1973).

33.) R. L. Mowery, J. C. Miller, E. R. Krausz, P. N. Schatz, S. M. Jacobs, and L. Andrews, J. Chem. Phys., 70, 3920 (1979).

34.) W. J. Balfour, J. Chem. Ed., 56, 542 (1979).

35.) Bruce S. Ault, J. Amer. Chem. Soc., 102, 3480 (1980).

36.) Y. Tanaka, S. C. Davis, and K. J. Klabunde, J. Amer. Chem. Soc., 104, 1013 (1982).

37.) Y. Imizu and K. J. Klabunde, Inorg. Chem., in press.

38.) Paul G. Jasien and Clifford E. Dykstra, J. Amer. Chem. Soc., 105, 2089 (1983).

39.) P. H. Barrett, M. Pasternak, and R. G. Pearson, J. Amer. Chem. Soc., 101, 222 (1979).

40.) G. A. Ozin and J. G. McCaffrey, Inorg. Chem., 22, 1397 (1983).

41.) R. H. Hauge, J. W. Kauffman and J. L. Margrave, J. Am. Chem. Soc., 102, 6005 (1980).

42.) Stephen C. Davis, Ph.D. Thesis, University of North Dakota, 1980.

43.) A. R. Wolter, J. of Applied Physics, 36, 2377 (1965).

44.) G. Sauerbrey, Z. Physik, 155, 206 (1959).

45.) G. A. Ozin, and M. Moskovits, "Cryochemistry", J. Wiley and Sons, New York, (1976) pg. 54.

46.) M. Moskovits, and J. E. Hulse, J. Chem. Soc., Faraday Trans., 2, 73, 471 (1977).

47.) J. B. Hopkins, P. R. R. Langridge-Smith, M. D. Morse, and R. E. Smalley, J. Chem. Phys., 78, 1627 (1983).

48.) P. L. Po, and R. F. Porter, J. Phys. Chem., 81, 2233 (1977).

49.) "Handbook of Chemistry and Physics," 60th ed.; CRC Press; Cleveland, Ohio, 1980, p. F220-224.

50.) P. S. Skell, E. M. Van Dam, and M. P. Silvon, J. Amer. Chem. Soc., 96, 626 (1974).

51.) M. Moskovits, and G. A. Ozin, "Cryochemistry", John Wiley and Sons, New York, (1976) p. 27.

52.) H. R. Rogers, C. L. Hill, Y. Fujiwara, R. J. Rogers, H. L. Mitchell, and G. M. Whitesides, J. Am. Chem. Soc., 102, 217 (1980).

ATOM VERSUS CLUSTER REACTIVITIES FOR CALCIUM AND MAGNESIUM

by

ALAN RAY WHETTEN

B.S., Fort Lewis College, 1982

AN ABSTRACT OF A MASTER'S THESIS

submitted in partial fulfillment of the

requirements for the degree

MASTER OF SCIENCE

Department of Chemistry

KANSAS STATE UNIVERSITY
Manhattan, Kansas

1984

ABSTRACT

Calcium and magnesium atoms, dimers, and larger clusters have been isolated under matrix isolation conditions. The reactivity of each of these species with alkyl halides is described in the present study. Ca atoms, Ca_2, $(Ca)_x$ and Mg atoms, Mg_2, Mg_3, Mg_4, and $(Mg)_x$ were codeposited with CH_4, CH_3F, CH_3Cl, CH_3Br, and CH_3I at 9K. UV-visible spectroscopic evidence indicates that M_2, M_3, M_4 and $(M)_x$ were the reacting species to form $CH_3(M)_nX$ type products, where n>1. An electron transfer mechanism is proposed and is made possible by the lower ionization potential of clusters. Thermodynamic and kinetic considerations as well as bond strengths, crystal lattice structures and theoretical calculations are presented as rationale for the greater reactivity of metal clusters and the stability of the cluster Grignard product.